Current Research in Food Science 5 (2022) 1167–1175

Contents lists available at ScienceDirect

Current Research in Food Science

journal homepage: www.sciencedirect.com/journal/current-research-in-food-science

Saponins from bitter melon reduce lipid accumulation via induction of autophagy in *C. elegans* and HepG2 cell line

Juan Bai [a,b], Ying Zhu [a], Linzhao He [a], Jinfu Zhang [a], Jie Li [a], Ruirong Pan [a,c], Jiayan Zhang [a], Yansheng Zhao [a], Lin Cui [a], Haina Lu [a], Ya Jiang [b], Xiang Xiao [a,b,*]

[a] School of Food and Biological Engineering, Jiangsu University, Zhenjiang, 212013, China
[b] Jiangsu Jiangnan Biotechnology Co. LTD, Zhenjiang, 212013, China
[c] Department of Endocrinology, Affiliated Hospital of Jiangsu University, Zhenjiang, 212013, China

ARTICLE INFO

Handling editor: Quancai Sun

Keywords:
Bitter melon saponin
Fat accumulation
Lipidomics
Autophagy
Daf-16/ hlh-30

ABSTRACT

Saponins from bitter melon (BMS) are well-known to have various biological activities, especially in the field of fat-lowering. However, many gaps remain in our knowledge of BMS-induced fat reduction and health benefits. Here, we aimed to investigate the precise mechanism of BMS in alleviating fat accumulation in *C. elegans* and HepG2 cell line. Results indicated that BMS showed strong fat-lowering and lifespan-extension properties. Lipidomic analysis illustrated that BMS could alter the lipid profile, especially represented by phosphatidylethanolamine (PE) increase, which plays an essential role in autophagy. Furthermore, we applied gene-deficient mutants and RNAi technology to confirm that BMS largely depended on *daf-16*/FoxO1 and *hlh*-30/TFEB mediated lipophagy to reduce fat deposition. In addition, BMS could ameliorate oil acid (OA)-induced fat accumulation in HepG2 cells by induction of autophagy-related proteins, such as the phosphorylated AMPK and LC3B. In conclusion, our results elucidated the underlying mechanism of bitter melon saponins interfering with lipid metabolism from the autophagy point of view, which provide new insights into a nutraceutical to mitigate obesity.

1. Introduction

Bitter melon (*Momordica charantia* L.) is recognized as a medicinal and edible plant for obesity and diabetes prevention due to its numerous active ingredients, like polysaccharides, saponins, peptides or flavonoids (Bai et al., 2018). Saponins, the main source of bitter taste in bitter melon, are reported to hold similar hypoglycemic property with insulin, and the underlying mechanisms include the activation of AMPK and insulin receptor-1 (IRS-1), promotion of downstream glucose transporter (GLUT4), or elevation of intracellular glycogen synthase kinase-3 β (GSK-3β) (Han et al., 2018; Tan et al., 2016). In addition, BMS could inhibit the differentiation of preadipocytes by down-regulating PPARγ in 3T3-L1 preadipocytes, and effectively reduce plasma lipid levels in rat (Senanayake et al., 2012). However, the detailed mechanism of BMS in fat-lowering effect remains elusive.

Caenorhabditis elegans (*C. elegans*), a whole-organism, has recently gained considerable interest in studying the molecular mechanism of lipid metabolism and aging due to their short lifespan, broad availability of mutants and ease of genetic manipulation (Bai et al., 2021). Commonly, researches in the *C. elegans* lipid field have been ongoing to characterize lipid biosynthetic genes, regulatory genes affecting lipid synthesis, storage, and breakdown with some specific lipids alteration, such as triacylglycerol (TAG), phosphatidylethanolamine (PE), or phosphatidylcholine (PC), which are considered crucial for membrane integrity and signaling pathways (Kimura et al., 2016). In order to identify and quantify the lipid species relevant for various biological processes, lipidomic technologies have been largely used to characterize the lipid profile of *C. elegans*, through the analysis of structure, function, or interaction of cellular lipids, which also play an essential role in nutritional research (Kim et al., 2019).

In the process of lipid hydrolysis, the lipid autophagy (i.e. lipophagy) connects autophagy and lipid metabolism, equally important as lipolysis. Lipid droplets (LDs) are cytoplasmic organelles containing mostly TAG, surrounded by a monolayer mainly of PC and PE. AMPK (homolog of *aak-2* in *C. elegans*) is an energy sensor modulating fat catabolism, including fatty acid oxidation, lipolysis and autophagy. Adipose

* Corresponding author. School of Food and Biological Engineering, Jiangsu University, Zhenjiang, 212013, China
E-mail address: xiaoxiang1@aliyun.com (X. Xiao).

https://doi.org/10.1016/j.crfs.2022.06.011
Received 12 April 2022; Received in revised form 22 June 2022; Accepted 27 June 2022
Available online 22 July 2022

Triglyceride Lipase (ATGL) is a well-known cytosolic lipase to break down TAG into FFAs and glycerol, which means lipolysis (Obrowsky et al., 2013; Li et al., 2022). Except for lipolysis, LDs can also be accessed by lipophagy, a specific subset of selective autophagy that catabolizes the components of LDs. Lipophagy-associated genes are primarily controlled by the master regulator of lysosomal biogenesis transcription factor EB (TFEB)/helix-loop-helix (*hlh*)-30, the forkhead homeobox transcription factor FoxO1/*daf-16* as well, which are required for LD clearance in multiple systems (Gary et al., 2015).

In order to investigate the precise mechanism of BMS inhibiting fat accumulation, we applied the lipidomics to uncover another pathway additive to that of fat synthesis. As expected, the lipidomic analysis predicted that autophagy was involved in the effects of BMS, characterized by the regulation of *daf*-16/hlh-*30* mediated lipophagy. In addition, BMS increased the level of autophagy in HepG2 cell lines with OA treatment. This study can enrich the mechanism of the biological activity of bitter melon saponins, and provide potential applications in the field of food nutrition.

2. Materials and methods

2.1. Chemicals and reagents

Fresh bitter melons were collected from Lvjian Agricultural Station (Yangzhong City, China) and authenticated by Jiangsu Academy of Agricultural Science. HepG2 cell was purchased from Shanghai institute of biochemistry and cell biology. Oil Red O staining, triglyceride (TG) reagents and protein assay kit were purchased from Nanjing Jiancheng Bioengineering Institute (Nanjing, China). Levamisole hydrochloride and chemicals for *C. elegans* cultivation were purchased from Shanghai Alighting Biochemical Technology Co., LTD (Shanghai, China). Reagents for qRT-PCR were from Takara Bio Inc. (DaLian, China).

2.2. BMS preparation and chemical constituents analysis

Fresh and unripe bitter melons were washed thoroughly and the seeds were removed. After sliced thinly, bitter melon slices were frozen-dried and milled to the powder (diameter < 105 μm). BMS was prepared as previously described (Bai et al., 2020b), as the following: the milled powder was added with 75% ethanol for reflux extraction twice at 80 °C, and the filtrate was collected. Then n-butanol saturated with water was applied to extract from the filtrate for 3 times until the concentrated n-butanol phase was brown and sticky. Then methanol and acetone were added to produce precipitation, which was lyophilized as the BMS. In our study, the saponin content in the stocking solution dissolved by ethanol was 54.60 μg/mL ginsenoside Rg1 equivalent detected by vanillin–acetic acid method (Lin et al., 2020). Stock solution of BMS was prepared in ethanol at 10 mg/mL and stored at −20 °C.

Next, we applied ultra-high performance liquid chromatography tandem with high resolution mass spectrometry (UPLC-HRMS) (Thermo-Fisher Scientific, USA) to analyze the components, following the previous literature (Zhao et al., 2021). Using ginsenoside Rg1 as internal standard, 7 main components of saponins from bitter melon were identified (Figure S1 A). Most of the saponins were cucurbitane triterpenoids, including momordicosides P (RT=7.312) and L (RT=1.081), Kuguacin N (RT=9.065) and momordicine I (RT=8.397). The basic structure of cucurbitane aglycone was preliminarily drawn (Figure S1 B).

2.3. C. elegans strains and cultivation

Escherichia coli OP50 and *C. elegans* strains including N2, Bristol (wild type), CF1038 (*daf-16* (mu86)), JIN1375 (*hlh-30* (tm1987) IV), TJ356 (DAF-16:GFP), DA2130 (LGG-1:GFP) were obtained from Caenorhabditis Genetics Center (CGC) (Minneapolis, MN, USA). Worms were propagated on nematode growth medium (NGM) spread with *E. coli* OP50 bacterial. Experiments were performed at 20 °C. L1 worms were synchronized by using bleach and NaOH according to previously describe (Bai et al., 2020a), which were applied in all assays. Synchronized L1 worms were supplemented with ddH_2O as control or BMS (100 μg/mL or 200 μg/mL, final concentrations) mixed with *E. coli* OP50 on NGM plate.

2.4. Oil red O (ORO) staining and TG assay

Synchronized L1 worms were treated with BMS from L1 to late L4 stage. After 48 h, 300-500 adult worms in each group were washed with M9 buffer for three times, followed by fixation and dehydration with 60% isopropanol for 15 min. ORO stocking solution (5 mg/mL) was diluted with ddH_2O to 60% working solution and filtered to dye the fixed worms for 2 h at room temperature. Next, worms were washed with M9 three times to remove the extra dye, then mounted and imaged with a microscope outfitted with DIC optics (Leica, Wetzlar, Germany). Image J was used to quantify the ORO intensities (Xiao et al., 2020a).

For TG quantification, worms (~1000 worms each group) were washed from NGM for three times with M9 buffer to collect worm pellets, and homogenized using ultrasonic disruption to release the triglyceride, followed by centrifugation at 8000 rpm for 5 min to obtain the supernatant for TG assay. TG content was normalized by the protein content, which was determined according to the instructions of Coomassie brilliant blue kit.

2.5. Body size, locomotive activity, growth rate and lifespan assay

Worm sizes were represented by the body length and width. *C. elegans* were treated with BMS from L1 to L4 larvae. Photographs were taken of the worms after anesthetization by 100 μM levamisole hydrochloride. The body length and body width of each worm (more than 30 worms) was quantified by using Image J software. The test was performed at least 3 times.

For locomotive behavior, head thrashes and body bends were assessed. *C. elegans* were treated with BMS from L1 to L4 larvae. For thrashing frequency of the head, the head of worms from one side to the other and then back within 1 min on clean NGM was recorded under a stereo microscope. For the frequency of body bends, worms placed on a NGM without *E. coli* forwarded body walks in a shape of wavelength, and the number of wavelength shapes within 1 min worms were recorded. Twenty nematodes in each group were examined per experiment. For the growth rate, the number of worms at each developmental stage after 48 h was counted ($n > 100$ worms per group) as previously described (Shen et al., 2017).

Lifespan assay was performed at 20 °C as previously described (Bai et al., 2020a). L1 worms were cultivated to L4 stage on NGM and then transferred to the Transwell®-24 well permeable plates (BD Biosciences Inc., NY, USA) supplemented with ddH_2O or BMS (100 and 200 μg/mL) and 2% glucose. Fluorodeoxyuridine (FUDR, 120 mM) was added to prevent eggs from hatching after worms reached L4 stage/young adult stage during the treatment period. The medium was changed every two days. Survivals were recorded every other day until all the worms died. The day when we treated the L4 worms was defined as day 0 of adult age.

2.6. Detection of proteins with GFP labeled expressions

Synchronized transgenic worms and DAF-16:GFP (TJ356) and DA2130 (LGG-1:GFP) were treated with BMS for 48h (~500 worms per each group), then anesthetized with 100 μM levamisole hydrochloride at room temperature and put onto a glass slide. Images were captured by an Olympus IXplore (Olympus Sales Service Co., Ltd. Beijing, China) fluorescence microscope equipped with a GFP (emission 500–515 nm) filter (10 × magnification). Three independent experiments were performed. Quantification of fluorescence intensity was evaluated with the

ImageJ (NIH) software to measure the percentage of GFP-positive nuclei in transgenic worms.

2.7. Lipidomic profiling by LC-MS/MS and data analysis

For lipidomics, worms (~10000 worms each duplicate, 6 replicates per group) were transferred from NGM and washed five times with M9 buffer to collect worm pellets. 480 μL extract solution (MTBE: MeOH= 5: 1) was added sequentially, then homogenized at 35 Hz for 4 min (Ultra-Turraz homogenizer IKA LaborTechinik) and sonicated for 5 min (IKA LaborTechnik) in ice-water bath, which were repeated for 3 times. Then the samples were incubated at −40 °C for 1 h and centrifuged at 3000 rpm for 15 min at 4 °C. 300 μL of supernatant was transferred to a fresh tube and dried in a vacuum concentrator at 37 °C. Then, the dried samples were reconstituted in 200 μL of 50% methanol in dichloromethane by sonication for 10 min in ice-water bath. The constitution was then centrifuged at 13000 rpm for 15 min at 4 °C, and 75 μL of supernatant was transferred to a fresh glass vial for LC/MS analysis. The quality control (QC) sample was prepared by mixing an equal aliquot of the supernatants from all of the samples.

The UHPLC separation was carried out using an ExionLC Infinity series UHPLC System (AB Sciex), equipped with a Kinetex C18 column (2.1 * 100 mm, 1.7 μm, Phenomen). The mobile phase A consisted of 40% water, 60% acetonitrile, and 10 mmol/L ammonium formate. The mobile phase B consisted of 10% acetonitrile and 90% isopropanol, which was added with 50 mL 10 mmol/L ammonium formate for every 1000 mL mixed solvent. The analysis was carried with elution gradient as follows: 0–12.0 min, 40%–100% B; 12.0–13.5 min, 100% B; 13.5–13.7 min, 100%–40% B; 13.7–18.0 min, 40% B. The column temperature was 55 °C. The auto-sampler temperature was 6 °C, and the injection volume was 2 μL (pos) or 4 μL (neg), respectively.

The TripleTOF 5600 mass spectrometer was used for its ability to acquire MS/MS spectra on an information-dependent basis (IDA) during an LC/MS experiment. In this mode, the acquisition software (Analyst TF 1.7, AB Sciex) continuously evaluates the full scan survey MS data as it collects and triggers the acquisition of MS/MS spectra depending on preselected criteria. In each cycle, the most intensive 12 precursor ions with intensity above 100 were chosen for MS/MS at collision energy (CE) of 45 eV (12 MS/MS events with accumulation time of 50 msec each). ESI source conditions were set as following: Gas 1 as 60 psi, Gas 2 as 60 psi, Curtain Gas as 30 psi, Source Temperature as 600 °C, Declustering potential as 100 V, Ion Spray Voltage Floating (ISVF) as 5000 V or −3800 V in positive or negative modes, respectively.

With the MS/MS spectrum, lipid identification was achieved through a spectral match using LipidBlast library. Dataset containing the information of peak number, sample name and normalized peak area was imported to SIMCA16.0.2 software package (Sartorius Stedim Data Analytics AB, Umea, Sweden) for multivariate analysis, including principle component analysis (PCA), orthogonal projections to latent structures-discriminate analysis (OPLS-DA). The value of variable importance in the projection (VIP) of the first principal component in OPLS-DA analysis was obtained. It summarizes the contribution of each variable to the model. The metabolites with VIP>1 and $p<0.05$ (student *t*-test) were considered as significantly changed metabolites. In addition, commercial databases including KEGG (http://www.genome.jp/kegg/) and MetaboAnalyst (http://www.metaboanalyst.ca/) were used for pathway enrichment analysis.

2.8. Quantitative real time reverse-transcription PCR (qRT-PCR)

Total RNA of worms (~3000 worms per sample) was extracted by a TaKaRa MiniBEST Universal RNA extraction kit (Takara Bio, DaLian, China), which was reverse-transcribed to cDNA using a PrimeScript RT Master Mix kit (Takara Bio, DaLian, China). Quantification of gene expression by real-time PCR conducted on a CFX96 real-time PCR detection system (BioRad, California, America) based on the SYBR Premix Ex Taq kit (Takara Bio, DaLian, China). Primer sequences used in this study were listed in Table S1, and *act-1* was used as an internal control. Quantitative PCR amplification for all of the genes included pre-incubation at 95 °C for 10 s, followed by 40 cycles at 95 °C for 5 s, and 95 °C for 30 s, and then calculation of the fold change by the $2^{-\Delta\Delta Ct}$ method (Xiao et al., 2020b).

2.9. RNA interference (RNAi)

E. coli HT115 (DE3) harboring empty vector L4440 or expressing double stranded RNA corresponding to *hlh-30* was transferred into LA broth containing isopropyl 1-thio-β-d-galactopyranoside (IPTG, 5 mM). L1-larvae were fed with *E. coli* HT115 carrying double stranded RNA for *hlh-30* gene or harboring empty vector L4440 as the control (Yang et al., 2020). Once they developed into gravid, worms were transferred to a fresh RNAi plate to lay eggs and obtain the second generation for treatment of BMS. The primer of *hlh-30* for RNAi was forward: CCGCTCGAGTCTTCCCATCTATTCACGGC; Reverse: CCCAAGCTTC TCTGATGTGTTCTTCGGCA. qRT-PCR was employed to confirm the RNAi efficiency (Fig. S3).

2.10. HepG2 cell culture and western blotting analysis

The cells were cultured in monolayers up to 80% confluence in DMEM supplemented with 10% heat-inactivated fetal calf serum and 1% penicillin/streptomycin at 37 °C in a humidified incubator supplied with 5% CO_2. Cells in the logarithmic growth phase were used for all the studies described below. 0.5 mM oleic acid (OA)was used for 24 h to induce fat accumulation of HepG2 cells as the model group (Song et al., 2022), and BMS was treated for another 24 h.

Proteins of HepG2 cells were extracted by RIPA lysate with protease and phosphatase inhibitors (Beijing Solarbio Science & Technology Co., Ltd., Beijing, China) and centrifuged at 12000 rpm for 20 min to obtain the supernatant. Protein concentrations were determined by BCA assay kit (Nanjing Jiancheng Bioengineering Institute, Nanjing, China). Briefly, the lysate in loading buffer (30 μg protein/lane) was separated by sodium dodecyl sulfate polyacrylamide gel electrophoresis (SDS-PAGE) and transferred to a polyvinylidene fluoride (PVDF) membrane. The membranes were then blocked and probed with antibodies against AMPK, p-AMPK, LC-3B and β-actin (Cell Signaling Technology, Inc., USA), and incubated with the membranes at 4 °C overnight. Bands were detected using electrochemiluminescence (ECL) reagents (Millipore) according to the manufacturer's instructions. All primary and secondary antibodies were obtained from Abcam (Abcam, Cambridge, MA). Quantity One software (BioRad) was used to quantify band densities.

2.11. Statistical analysis

All data were expressed as means ± standard error (SE). Statistical analysis was performed using one-way analysis of variance, followed by Tukey's multiple range test to compare between groups. The significance of differences was defined at the $p < 0.05$ level.

3. Results and discussion

3.1. BMS decreased fat accumulation and extended lifespan in C. elegans

To understand the function of BMS in lipid metabolism, we firstly estimated the effect of BMS on fat deposition in *C. elegans* judged by ORO. As shown in Fig. 1A and B, the dosages of 100 and 200 μg/mL BMS we have reported (Bai et al., 2020b) could profoundly decrease the overall fat compared to the control group, accompanied by the reduction of TG content. Consistent with the study of Lin et al. (2020), the inhibitory effects of momordica saponins extracts on fat accumulation in *C. elegans* were also observed.

Since lipid metabolism is linked to changes in physiology, the growth

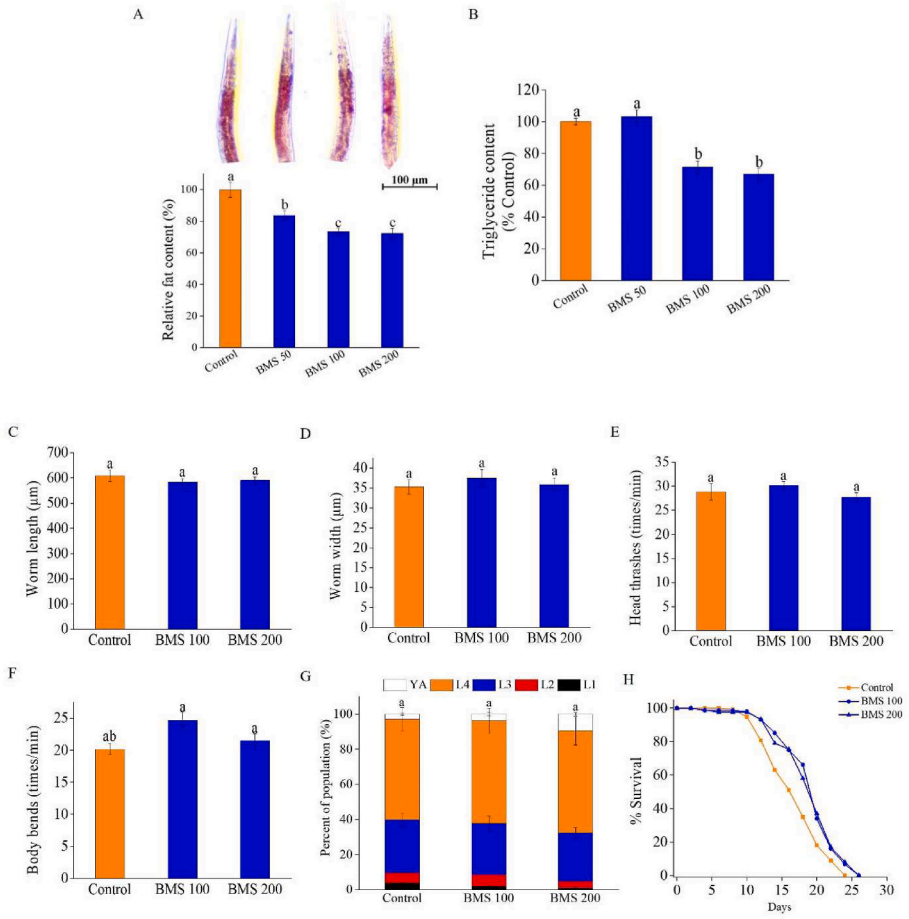

Fig. 1. Effects of BMS on overall fat accumulation and physiological indicators in wild-type (N2) *C. elegans*. Groups were divided into Control, BMS at 50 μg/mL, 100 μg/mL and 200 μg/mL, respectively. Worms were treated from L1 to L4 stage for 48 h followed by ORO staining (A) and TG assay (B). Fat intensities were analyzed by Image J from 15 to 20 worms (n = 3 sets/group). For the impacts of BMS on worm size, locomotive activities, growth rate and lifespan, L1 worms were treated with BMS (100 μg/mL and 200 μg/mL) for 48 h. Worm length(C) and worm width (D) were analyzed by Image J software (n > 30 worms per group). Head thrashes(E) and body bends (F) were counted under a microscope for 30 s (n > 30 worms per group). (G) The total number of worms at each developmental stage was counted (n > 100 per group). YA: young adult. (H) Lifespan was conducted from late L4 and the number was counted until all dead (Control, n = 126; BMS 100, n = 108; BMS 200, n= 138). Data were expressed as mean ± S.E. Different letters (a–b) denote meant values that were statistically different at $P < 0.05$.

and the survival of *C. elegans* (Sun et al., 2016), we next determined whether BMS treatment we used affected worm size, locomotive behavior, growth rate and lifespan. Results indicated that BMS at both 100 and 200 μg/mL showed no effects on worm length and width, the locomotive activities as an indicator of energy expenditure including head thrashed and body bends as well (Fig. 1C–F). In addition, no significant effects were observed in the growth rate of worms treated with BMS (Fig. 1G). Surprisingly, worms treated with 100 and 200 μg/mL BMS exhibited anti-aging characterized by increased mean lifespan by 16.64% and 13.83% (Fig. 1H and Table 1, $p < 0.001$), respectively. In accordance with Lin's findings (Lin et al., 2020), the ability of momordica saponins extracts improving lifespan was attributed to the stress resistance effect. Beyond that, we speculated that the altered lipid metabolism by BMS could make an essential impact on the extension of longevity, in which the mechanism needed further confirmation.

3.2. *Differential metabolites of lipidomics predicted autophagy may be a key pathway involved in the fat-lowering effects of BMS*

In *C. elegans*, animal development, metabolism, and lifespan are complexly connected with lipid molecules, which are regarded essential for signaling pathways and membrane integrity (Kimura et al., 2016). Herein, after confirmation of the fat-lowering impact of BMS, we further conducted the lipidomics to overview the effects of 100 μg/mL BMS on the profile of lipids in *C. elegans*. In all, 1190 and 1245 metabolites with identified names were detected in the positive and negative ion modes,

Table 1
Effects of BMS on survival rate in *C. elegans*.

Strains	*BMS* (μg/mL)	*No. Animals*	*Median Lifespan (days)*	*Mean lifespan (days±SE)* [a]	*MaximumLifespan (days)*	*P-value* [b]
N2	0	126	18	17.07 ± 0.35	24	< 0.001
	100	108	20	19.91 ± 0.36	26	
	200	138	20	19.43 ± 0.35	26	< 0.001
daf-16	0	160	8	8.81± 0.3	18	
	100	144	6	7.13± 0.2	18	<0.0001
hlh-30	0	160	12	11.71±0.46	26	
	100	129	12	12.14±0.47	26	0.8026
hlh-30 (RNAi)	0	110	20	18.02±0.5	26	
	100	109	14	14.99±0.57	26	0.0009

Worms were treated with BMS from the late L4 stage. FUDR (120 μM) was added to sterilize the worms during the treatment period. Survivals were recorded every other day until all of the worms died.

[a] The mean lifespan was referred to the exact time when the survival rate reached to 50%, which was generated by the OASIS application.

[b] P-values were analyzed by log-rank (Mantel-Cox method) tests. Significant differences were defined at $p < 0.05$.

respectively (Fig. S2). OPLS-DA was applied to examine changes in lipid metabolites patterns between the control and BMS groups as well as identify key metabolites that contributed to metabolic pattern changes. OPLS-DA indicated that the two groups formed clear clusters based on the lipids in both positive and negative modes (Fig. 2A and B), and the cross-validation showed that the original model had good robustness and there is no overfitting phenomenon ($R^2 = 0.995$, $Q^2 = 0.455$ in positive; $R^2 = 0.990$, $Q^2 = 0.365$).

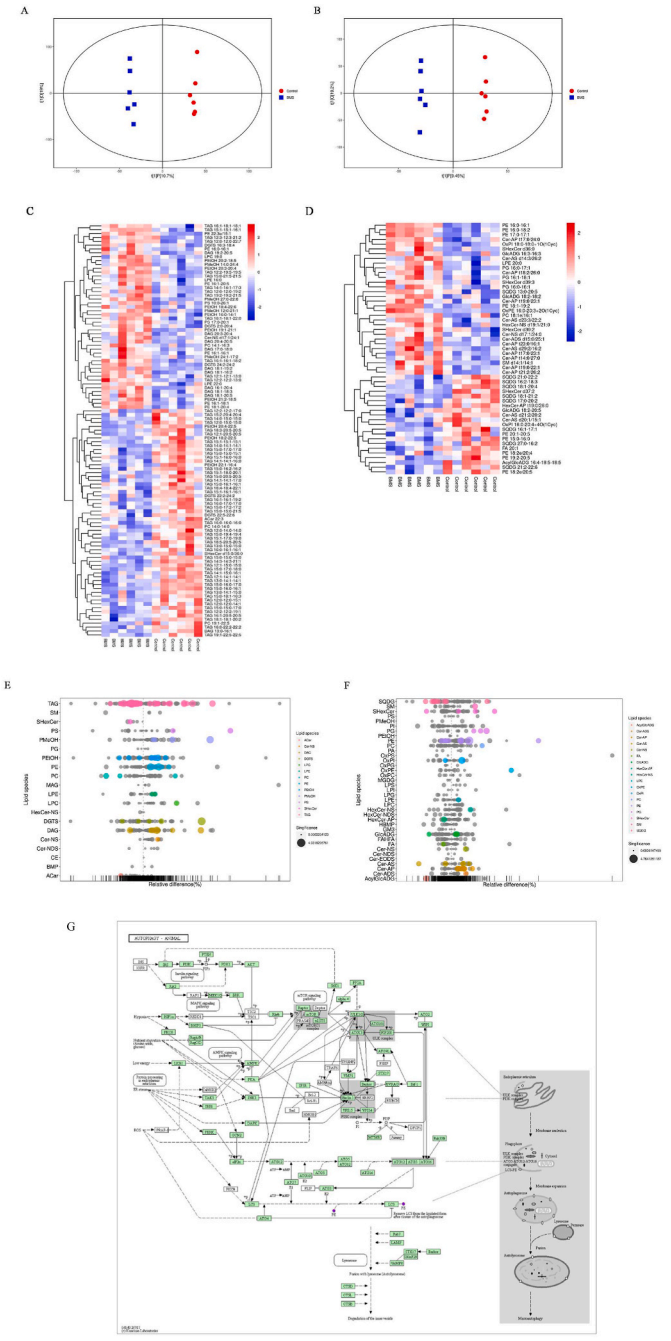

Fig. 2. Lipidomics analysis of C. elegans treated with BMS. L1 worms (~10000 worms each duplicate, 6 replicates per group) were treated with BMS (100 μg/mL) for 48 h. (A) OPLS-DA plots in positive ion mode, (B) OPLS-DA plots in negative ion mode, (C) Heatmaps in positive ion mode, (D) Heatmaps plots in negative ion mode, (E) Bubble plots in positive ion mode, (F) Bubble plots in negative ion mode (dots in grey indicated metabolites without significance), and (G) PE involved autophagy pathway in KEGG analysis (PE was indicated as purple dots). (For interpretation of the references to colour in this figure legend, the reader is referred to the Web version of this article.)

All the lipid signals in the mode of positive and negative ion, identified as significant (VIP>1 and $p<0.05$), were depicted in Fig. 2C and D, as the heatmaps. The heatmap provided an overview of the lipids signals and their abundance, in terms of overexpression (in red) or under expression (in blue). For positive ion mode, compared with the control group, 107 identified lipids were significantly affected by BMS treatment, in which 58 lipids were downregulated and 49 lipids were upregulated (Table S2). For negative ion mode, 53 identified lipids were altered by BMS, in which 33 were increased and 20 were declined (Table S3). In general, these lipids belonged to species like triacylglycerol (TAG), phosphatidylethanolamine (PE), Phosphatidylcholine (PC), phosphatidylserine (PS), phosphatidylethanol (PEtOH), lysophosphatidylethanolamine (LPE) and so on.

In regard to the TAG, more kinds of TAG concentration were higher in the control group (Fig. 2C and E), which was in line with the decreased TG content in the BMS group (Fig. 1B), confirming the lipid-lowering effect of BMS. Moreover, the majority of TAG showed reduced concentration levels in the BMS group with most of them being significant in particular in an unsaturated state, such as TAG 16:1–18:1–18:1, TAG 16:1–16:1–18:2, TAG 15:1–15:1–16:1, TAG 19:2–19:2–21:5 and so on. By contrast, TAG in a saturated state, like TAG 15:0–15:0–15:0, TAG 16:0–16:0–16:0, TAG 15:0–15:0–17:0, and TAG 15:0–16:0–17:0, were notably lower in the BMS group compared with the control group (Fig. 2C and Table S2). As we all know, the World Health Organization recommends that people limit saturated fat consumption because of its proven link to cardiovascular disease. High saturated fat can lead to problems such as elevated cholesterol, atherosclerosis, and increases LDL levels, while unsaturated fats can raise HDL levels (Sacks et al., 2017). A recent and compelling meta-analysis of lipid composition revealed that the energy-related lipids, such as TAG, were more likely to be in an unsaturated state in the long-lived species (Bozek et al., 2017). Therefore, we speculated that the higher unsaturated lipid brought about the prolonged lifespan in the BMS group, which needed to be investigated more in the future.

With respect to the PE, we surprisingly observed that all the differentiated PE species were increased in positive ion mode (Fig. 2C and E), especially the PE 16:1–16:1, PE 16:1–18:1 and PE 16:0–16:1 (Table S2). In addition, PE species with high significances in negative ion mode were also upregulated by BMS (Figs. 2D and 3F). PE is one of the most abundant phospholipids with both structural and metabolic functions in cells. Supplementation with PE confers anti-oxidant and anti-aging effects via reducing insulin/IGF-1-like signaling pathway in *C. elegans* (Sp et al., 2021). Lowering cellular PE cause α-synuclein accumulation, a protein causing dopaminergic neuronal death in Parkinson's disease (PD) (Wang et al., 2014). What's more, a meta-analysis study has revealed that structural lipids like PE and PS are more likely to be found in a saturated state in the long-lived species (Bozek et al., 2017), which implying that higher levels of PE 16:1–16:1, PE 16:1–18:1 and PE 16:0–16:1 in the BMS group played a vital role in the lifespan-extension effect of BMS. Since the relevance between PE and the aging, follow-up studies should be conducted to expand our findings.

KEGG was carried out to map the corresponding pathways of differential metabolite and we further screened to find the key pathways with the highest correlation with differentially expressed lipids (Table 2), i.e., metabolic pathways, glycerophospholipid metabolism, autophagy and glycosylphosphatidylinositol (GPI)-anchor biosynthesis. Among the key pathways, we were excited to find the predicted autophagy pathway involved in either positive or negative ion mode, which was attributed to the PE elevation. It's well known that autophagy is an evolutionarily conserved, lysosome dependent catabolic process, regulating cellular energy as well as lipid, glucose and amino acid metabolism to maintain cellular homeostasis, which has been proven to be a target for combating obesity (Zhang et al., 2018). Furthermore, autophagy and lipid metabolism can coordinately modulate lifespan (Hansen et al., 2011).

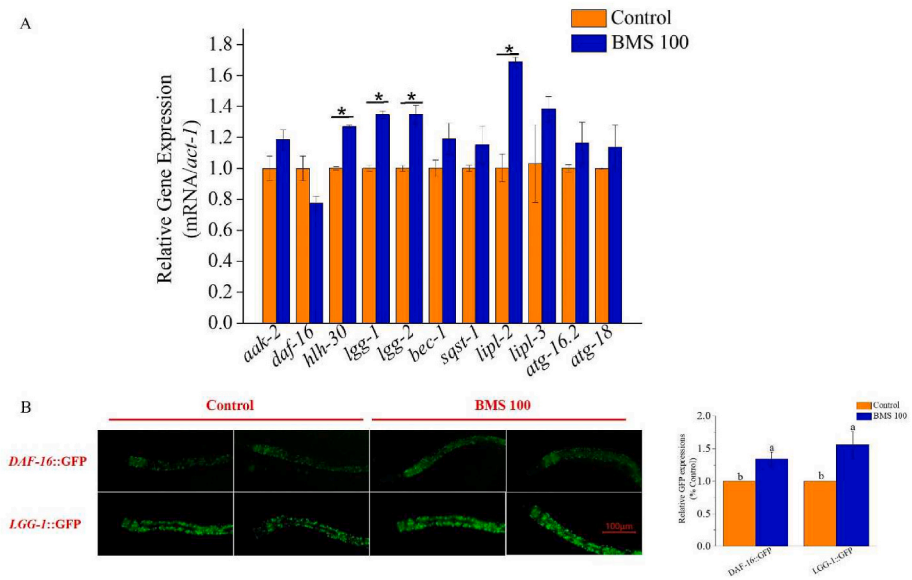

Fig. 3. BMS altered lipophagy-related genes and proteins levels. L1 worms were supplemented with BMS (100 μg/mL) for 48 h in *N2*, GFP-labeled worms. (A) BMS regulated the mRNA levels of lipophagy-related genes. (B) BMS enhanced the expression of DAF-16 and LGG-1 proteins.

Table 2
KEGG pathway annotation information.

KEGG pathways	Compounds
cel01100 Metabolic pathways - C. elegans (nematode)	cpd:C00350 Phosphatidylethanolamine; cpd:C00157 Phosphatidylcholine; cpd:C00422 Triacylglycerol
cel00564 Glycerophospholipid metabolism - C. elegans (nematode)	cpd:C00157 Phosphatidylcholine; cpd:C00350 Phosphatidylethanolamine
cel04140 Autophagy - animal - C. elegans (nematode)	cpd:C00350 Phosphatidylethanolamine
cel00563 Glycosylphosphatidylinositol (GPI)-anchor biosynthesis - C. elegans (nematode)	cpd:C00350 Phosphatidylethanolamine

Lipophagy is a kind of selective autophagy of lipid droplets to regulate the intracellular storage and utilization of lipids whereby maintaining the lipid homeostasis. As shown in the overview of the autophagy pathways in *C. elegans* (Fig. 2G), during the process of lipophagy, PE functions as a vital anchor to autophagosomal membranes for the autophagy-related protein LGG (its mammalian orthologue LC3) in *C. elegans* via lipidation (Ichimura et al., 2000). And the expansion and closure of the autophagosome is regulated by the PE lipidated LGG. Studies have reported that the overall abundance of PE is critical for PE-lipidation of LC3/Atg8 and could thus regulate autophagosomal membrane formation (Rockenfeller et al., 2015). As we focused on the effects of BMS on lipid homeostasis, this finding prompted us to uncover whether BMS could induce lipophagy, thereby attenuating the fat accumulation and extending the lifespan as well, through increasing the level of PE.

3.3. BMS could act on daf-16/hlh-30 mediated lipophagy to confer fat-lowering benefit

Upon the above, we followed to determine the effects of BMS on the lipophagy and its potential mechanism. Fig. 3A illustrated the changes of lipophagy-related genes expressions by BMS treatment. *hlh-30* (TFEB homolog in mammalian), *lgg-1* (LC3B-I homolog), *lgg-2* (LC3B-II homolog) and *lipl-2* (LAL homolog) were all significantly up-regulated in BMS group ($p< 0.05$), while other related genes like *aak-2* (AMPK homolog), *daf-16* (FoxO1 homolog), *bec-1* (Beclin1 homolog), *sqst-1* (p62 homolog), *lipl-3* (LAL homolog), *atg-16.2* (ATG-16 homolog), and *atg-18* (ATG-18 homolog) showed no notable alterations, which partially implying BMS could regulate the lipophagy at the transcriptional level.

The forkhead homeobox type O1 (FoxO1) transcription factor is an important regulator of energy stress response in the lipophagy process, regulated by upstream AMPK. And transcription factor EB (TFEB) is also a major inducer of lysosomal biogenesis and autophagosome-lysosome fusion, negatively regulated by upstream mTORC1 (Kounakis et al., 2019). Both of them could induce lysosomal acid lipase (LAL) expression and promote autophagolysosomal-mediated lipid degradation and fatty acid β oxidation alone or in combination (Angelini et al., 2016; Gomaraschi et al., 2019). Recently, accumulating and emerging evidence indicated that FoxO1 and TFEB have been the targets to interfere with the autophagy process of lipid droplets to regulate lipid metabolism (Levine et al, 2019).

As shown in Fig. 3B, the protein level of *daf-16*/FoxO1 and LGG-1 was detected. Different from the mRNA level, the GFP-labeled *daf-16* was higher by the administration of BMS, indicating BMS acted on *daf-16* at post-transcriptional or translational level. Higher LGG-1 expressions were observed with BMS administration, consistent with the mRNA level, implying the level of autophagy was upregulated by BMS. We next used *daf-16* deficient-mutant to verify the fat-lowering property of BMS. Results showed that the effects of BMS on inhibiting fat accumulation was diminished in the *daf-16* mutant, concomitant with the abrogation of lifespan extension (Fig. 4A and D, Table 1), hinting *daf-16* was required in the BMS' fat-lowering and lifespan prolongation functions. Likewise, we applied *hlh-30* deficient mutant and silenced *hlh*-30/TFEB in *C. elegans* by RNAi to detect the role of *hlh-30* in the effects of BMS. Fig. 4B, C, E and F elucidated that deficiency and silence of *hlh-30* could totally abolish BMS' functions. Collectively, we concluded that both *daf-16*/FoxO1 and *hlh*-30/TFEB played essential roles in the induction of lipophagy by BMS supplement, whereby enhancing the lipid hydrolysis, decreasing the fat deposition and prolonging the lifespan.

It is known that there are two types of cellular lipid degradation, namely, lipases-mediated lipolysis and lipophagy. We confirmed that the *daf*-16/hlh-*30* mediated-lipophagy took effects in the process of BMS' fat-lowering function. Some natural functional components act as AMPK activators, like EGCG (Madeo et al., 2019), resveratrol (Milton et al., 2018) and cinnamaldehyde (Neto et al., 2019), can activate the

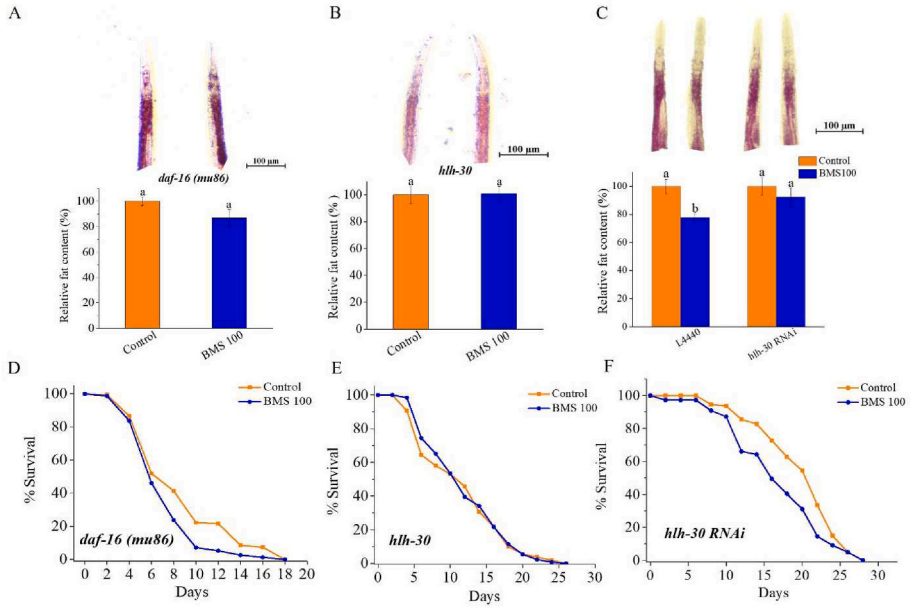

Fig. 4. Impacts of BMS on the *daf*-16/hlh-*30* mediated lipophagy pathway. L1 worms were supplemented with BMS (100 μg/mL) for 48 h in *daf-16* and *hlh-30* deficient mutants, and *hlh-30* interfered worms. Effects of BMS treatment on the fat accumulation in *daf-16* deficient mutant (A), *hlh-30* deficient mutants (B) and *hlh-30* interfered worms (C). The influences of BMS on the lifespan in *daf-16* deficient mutant (D) (Control, n = 160; BMS 100, n = 144), *hlh-30* deficient worms (E) (Control, n = 160; BMS 100, n = 129), and *hlh-30* interfered worms (F) (Control, n = 110; BMS 100, n = 109).

AMPK pathway in liver cells and improve the autophagy level, thereby reducing lipid accumulation. Alternatively, some functional factors work as mTOR inhibitors, both caffeine (Sinha et al., 2014) and quercetin (Liu et al., 2015) can inhibit mTOR signaling pathway and activate autophagy, thus reducing fat deposition in liver tissues of obese mice induced by high fat diet and improving lipid metabolism disorders. Little known about whether these functional components could regulate FoxO1/TFEB mediated-lipophagy to maintain lipid homeostasis while inducing autophagy. Recently, formononetin (Wang et al., 2019) and trehalose (Zhu et al., 2020) have been reported to activate AMPK, accompanied by inducing TFEB-mediated lysosomal production, promoting the fusion of autophagosome and lysosome, thereby enhancing lipophagy levels and alleviating lipid disorders. In the current study, we verified the pivotal roles of *daf-16*/FoxO1 and *hlh*-30/TFEB in the properties of BMS in *C. elegans*, further studies in the mammalian models need to be deeply investigated.

3.4. BMS could ameliorate OA-induced fat deposition via activating AMPK phosphorylation and LC3B expressions in HepG2 cells

In order to identify whether BMS reduced fat accumulation accompanied the induction of autophagy in *vitro*, we further checked the impacts of BMS on the level of autophagy-related proteins in HepG2 cells. As shown in Fig. 5A, OA caused much higher fat deposition in HepG2 cells compared the control, while BMS significantly decreased the overall fat, which further confirmed the fat-lowering effect of BMS. Meanwhile, we detected the phosphorylation level of energy sensor AMPK and the expression level of autophagy marker LC3B (Fig. 5B). As expected, the activation of AMPK phosphorylation and LC3B expressions were observed in BMS treatment group, compared with the model group, imply that BMS could stimulate autophagy to respond the OA-induced fat accumulation.

There are many important signal pathways in the regulation of autophagy process and the mammalian target of AMPK is the key regulator, which regulates the downstream autophagosome formation

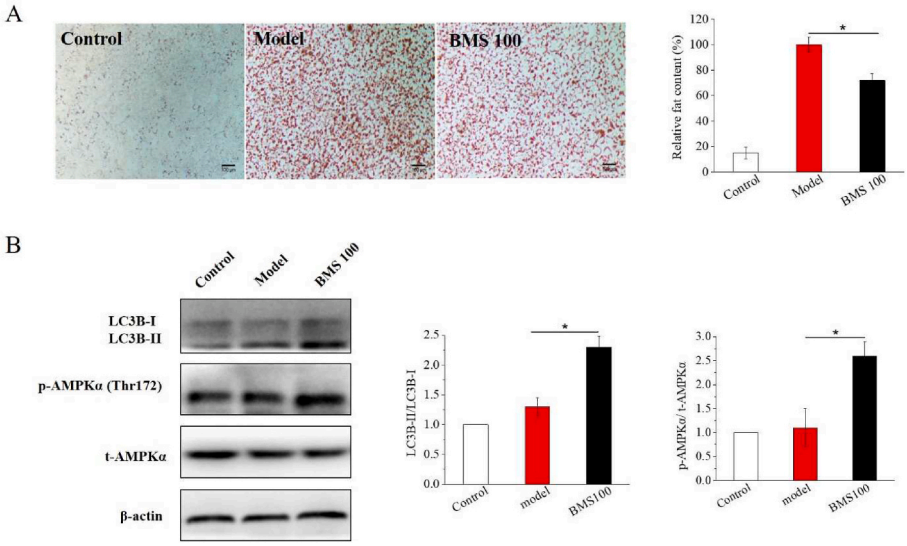

Fig. 5. BMS decreased OA-induced fat deposition in HepG2 cell via inducing autophagy. (A) BMS significantly decreased the overall fat of OA-induced fat accumulation by ORO staining. (B) BMS enhanced the phosphorylation of AMPK and increased the level of LC3B, an autophagy marker.

and fusion with the lysosome (He and Klionsky, 2009). In the process of autophagosome formation, LC3B-II serves as a good indicator. Increased LC3B-II levels are closely associated with activity of autophagy (Zeng et al., 2018). Some bioactive compounds such as berberine (Jin et al., 2017) and acetylshikonin (Zeng et al., 2018) could regulate the lipid metabolism by AMPK mediated pathway, accompanied by the increase of LC3B expression. In the resent study, higher expressions were observed with BMS administration, confirmed that BMS enhanced the autophagic function in the hepatocytes largely via activating AMPK.

4. Conclusion

In summary, our data indicated that saponins from bitter melon could inhibit fat accumulation in *C. elegans*. Lipidomic analysis revealed that BMS altered the lipid composition of the whole-organism, especially represented by the increased PE, which performed an important role in autophagy. Most of all, the *daf-16*/FoxO1 and *hlh*-30/TFEB mediated lipophagy were involved in fat-lowering and lifespan-extension effects of BMS. Meanwhile, BMS induced autophagy in OA-treated HepG2 cell via regulating p-AMPK and LC3B expressions. These novel findings may provide new insights into the molecular mechanisms underlying the action of bitter melon saponin in lipid metabolism and may aid in design of new therapies for intervention of obesity.

Funding sources

This work was supported by the China Postdoctoral Science Foundation (2020M671373), Jiangsu Postdoctoral Research Funding Program (2020Z070) and Jiangsu Agriculture Science and Technology Innovation Fund, CX(20)2036.

Declaration of competing interest

The authors declare that they have no known competing financial interests or personal relationships that could have appeared to influence the work reported in this paper.

Acknowledgements

Juan Bai (1039997619@qq.com) was the main executor of the experiment operation and paper writing. Ying Zhu (ying307@126.com), Linzhao He (1341037114@qq.com), Jinfu Zhang (3417309609@qq.com), Jie Li (1933718380@qq.com), Ruirong Pan (ruirong123@163.com), Jiayan Zhang (Jiayanzhang1988@163.com), Yansheng Zhao (zhaoys@ujs.edu.cn), Lin Cui (1932761349@qq.com), Haina Lu (1191716389@qq.com) and Ya Jiang (makio911@sina.cn) helped to do small parts of the experiments. Xiang Xiao (xiaoxiang1@aliyun.com) assisted me to form the framework of the experiment and revise the paper.

Appendix A. Supplementary data

Supplementary data to this article can be found online at https://doi.org/10.1016/j.crfs.2022.06.011.

References

Angelini, C., Nascimbeni, A.C., Cenacchi, G., Tasca, E., 2016. Lipolysis and lipophagy in lipid storage myopathies. BBA- Molecular Basis of Disease 1862, 1367–1373.
Bai, J., Farias-Pereira, R., Jang, M., et al., 2021. Azelaic acid promotes caenorhabditis elegans longevity at low temperature via an increase in fatty acid desaturation. Pharmaceut. Res. 38, 15–26.
Bai, J., Farias-Pereira, R., Zhang, Y., Jang, M., Park, Y., Kim, K., 2020a. C. elegans ACAT regulates lipolysis and its related lifespan in fasting through modulation of the genes in lipolysis and insulin/IGF-1 signaling. Biofactors 46, 754–765.
Bai, J., Zhu, Y., Dong, Y., 2018. Modulation of gut microbiota and gut-generated metabolites by bitter melon results in improvement in the metabolic status in high fat diet-induced obese rats. J. Funct.Foods 41, 127–134.
Bai, J., Zhu, Y., Li, J., Zhang, Y., Xiao, X., 2020b. Effects of bitter melon saponin on the glucose and lipid metabolism in HepG2 cell and C. elegans. J. Food Qual. 1–9, 2020.
Bozek, K., Khrameeva, E.E., Reznick, J., et al., 2017. Lipidome determinants of maximal lifespan in mammals. Sci. Rep. 7.
Gary, R., Rourke, O., Eyleen, J., 2015. MXL-3 and HLH-30 transcriptionally link lipolysis and autophagy to nutrient availability. Nat. Cell Biol. 17, 104.
Gomaraschi, M., Bonacina, F., Norata, G.D., 2019. Lysosomal acid lipase: from cellular lipid handler to immunometabolic target. Trends Pharmacol. Sci. 40, 104–115.
Han, J.H., Tuan, N.Q., Park, M.H., et al., 2018. Cucurbitane triterpenoids from the fruits of momordica charantia improve insulin sensitivity and glucose homeostasis in streptozotocin-induced diabetic mice. Mol. Nutr. Food Res. 62, 1700769.
Hansen, G., et al., 2011. Autophagy and lipid metabolism coordinately modulate life span in germline-less C. elegans. Curr. Opin. Struct. Biol. 21, 1507–1514.
He, C., Klionsky, D.J., 2009. Regulation mechanisms and signaling pathways of autophagy. Annu. Rev. Genet. 43, 67–93.
Ichimura, Y., Kirisako, T., Takao, T., et al., 2000. A ubiquitin-like system mediates protein lipidation. Nature 408, 488–492.
Jin, Y.L., Liu, S.P., Ma, Q.S., Xiao, D., Chen, L., 2017. Berberine enhances the AMPK activation and autophagy and mitigates high glucose-induced apoptosis of mouse podocytes. Eur. J. Pharmacol. 794, 106–114.
Kim, H.M., Long, N.P., Sang, J.Y., Anh, N.H., Kwon, S.W., 2019. Omics approach reveals perturbation of metabolism and phenotype in Caenorhabditis elegans triggered by perfluorinated compounds. Sci. Total Environ. 703, 135500.
Kimura, T., Jennings, W., Epand, R.M., 2016. Roles of specific lipid species in the cell and their molecular mechanism. Prog. Lipid Res. 62, 75–92.
Kounakis, K., Chaniotakis, M., Markaki, M., Tavernarakis, N., 2019. Emerging roles of lipophagy in health and disease. Front. Cell Dev. Biol. 7, 185.
Levine, B., Kroemer, G., 2019. Biological functions of autophagy genes: a disease perspective. Cell 176, 11–42.
Li, M.Q., Bao, X., Zhang, X.T., et al., 2022. Exploring the phytochemicals and inhibitory effects against α-glucosidase and dipeptidyl peptidase-IV in Chinese pickled chili pepper: insights into mechanisms by molecular docking analysis. LWT 162, 113467.
Lin, C.X., Chen, Y., Lin, Y.Z., Wang, X.B., Hu, L.Y., Cao, Y., Chen, Y.J., 2020. Antistress and anti-aging activities of Caenorhabditis elegans were enhanced by Momordica saponin extract. Eur. J. Nutr. 60, 1819–1832.
Liu, L., Gao, C., Yao, P., Gong, Z., 2015. Quercetin alleviates high-fat diet-induced oxidized low-density lipoprotein accumulation in the liver: implication for autophagy regulation. BioMed Res. Int. 1–9, 2015.
Madeo, F., Carmona-Gutierrez, D., Hofer, S.J., Kroemer, G., 2019. Caloric restriction mimetics against age-associated disease: targets, mechanisms, and therapeutic potential. Cell Metabol. 29, 592–610.
Milton, L.I., Aguirre, L., Etxeberria, U., et al., 2018. Involvement of autophagy in the beneficial effects of resveratrol in hepatic steatosis treatment. A comparison with energy restriction. Food Funct. 9, 4207–4215.
Neto, J., Boechat, S.K., Romo, J.S., Pazos-Moura, C.C., Oliveira, K.J., 2019. Treatment with cinnamaldehyde reduces the visceral adiposity and regulates lipid metabolism, autophagy and endoplasmic reticulum stress in the liver of a rat model of early obesity. J. Nutr. Biochem. 77, 108321.
Obrowsky, S., Chandak, P.G., Patankar, J.V., et al., 2013. Adipose triglyceride lipase is a TG hydrolase of the small intestine and regulates intestinal PPARα signaling. JLR (J. Lipid Res.) 54, 425.
Rockenfeller, P., Koska, M., Pietrocola, F., et al., 2015. Phosphatidylethanolamine positively regulates autophagy and longevity. Cell Death Differ. 22, 499–508.
Sacks, F.M., Lichtenstein, A.H., Wu, J.H., Appel, L.J., Horn, L.V.V., 2017. Dietary fats and cardiovascular disease a presidential advisory from the american heart association sacks. Circulation 136, e1.
Senanayake, G., Fukuda, N., Nshizono, S., et al., 2012. Mechanisms underlying decreased hepatic triacylglycerol and cholesterol by dietary bitter melon extract in the rat. Lipids 47 495–503.
Shen, P., Yue, Y., Kim, K.H., Park, Y., 2017. Piceatannol reduces fat accumulation in Caenorhabditis elegans. J. Med. Food 20, 887–894.
Sinha, R.A., Farah, B.L., Singh, B.K., 2014. Caffeine stimulates hepatic lipid metabolism by the autophagy-lysosomal pathway in mice. Hepatology 59, 1366–1380.
Song, J., Qiu, H.R., Du, P., et al., 2022. Polyphenols extracted from Shanxi-aged vinegar exert hypolipidemic effects on OA-induced HepG2 cells via the PPAR alpha-LXR alpha-ABCA1 pathway. J. Food Biochem. 46 (2), e14029.
Sp, A., Bkk, A., Skpa, B., 2021. Supplementation with phosphatidylethanolamine confers anti-oxidant and anti-aging effects via hormesis and reduced insulin/IGF-1-like signaling in C. elegans. Mech. Ageing Dev. 197, 111498.
Sun, Q., Yue, Y., Shen, P., Yang, J.J., Park, Y., 2016. Cranberry product decreases fat accumulation in Caenorhabditis elegans. J. Med. Food 19, 427–433.
Tan, S.P., Kha, T.C., Parks, S.E., Roach, P.D., 2016. Bitter melon (Momordica charantia L.) bioactive composition and health benefits: a review. Food Rev. Int. 32, 181–202.
Wang, S., Zhang, S., Liou, L.C., et al., 2014. Phosphatidylethanolamine deficiency disrupts α-synuclein homeostasis in yeast and worm models of Parkinson disease. Proc. Natl. Acad. Sci. U.S.A. 111, 3976–3985.
Wang, Y., Zhao, H., Li, X., Wang, Q., Li, P., 2019. Formononetin alleviates hepatic steatosis by facilitating TFEB-mediated lysosome biogenesis and lipophagy. J. Nutr. Biochem. 73, 108214.
Xiao, X., Tan, C., Sun, X., Zhao, Y., Zhou, X., 2020a. Fermented barley β-lucan regulates fat deposition in Caenorhabditis elegans. J. Sci. Food Agric. 100, 3408–3417.
Xiao, X., Zhang, X., Bai, J., et al., 2020b. Bisphenol S increases the obesogenic effects of a high-glucose diet through regulating lipid metabolism in Caenorhabditis elegans. Food Chem. 339, 127813.

Yang, Y., Shao, H., Wu, Q., Wang, D., 2020. Lipid metabolic response to polystyrene particles in nematode Caenorhabditis elegans. Environ. Pollut. 256, 113439.1-113439.9.
Zeng, J., Zhu, B., Su, M., 2018. Autophagy is involved in acetylshikonin ameliorating non-alcoholic steatohepatitis through AMPK/mTOR pathway. Biochem. Biophys. Res. Commun. 503, 1–6.
Zhang, Y., Sowers, J.R., Ren, J., 2018. Targeting autophagy in obesity: from pathophysiology to management. Nat. Rev. Endocrinol. 14, 356–376.
Zhao, Y.S., Wu, C., Zhu, Y., et al., 2021. Metabolomics strategy for revealing the components in fermented barley extracts with lactobacillus plantarum dy-1. Food Res. Int. 139, 109808.
Zhu, L., Yuan, Y., Yuan, L., Li, L., Cheng, J., 2020. Activation of TFEB-mediated autophagy by trehalose attenuates mitochondrial dysfunction in cisplatin-induced acute kidney injury. Theranostics 10, 5829–5844.